Combined effects of electron partial thermalization and secondary emission in Hall thruster discharges

E. Ahedo[a] and V. De Pablo
Universidad Politécnica de Madrid, Madrid 28040, Spain

(Received 19 March 2007; accepted 21 May 2007; published online 8 August 2007)

A model of the plasma interaction with the ceramic walls of a Hall thruster chamber is presented that takes into account partial thermalization of the electron distribution function. A model of secondary electron emission with both elastically reflected and true-secondary electrons is considered. The plasma response is found to differ substantially from low to high thermalization. The different roles of the bulk and emitted populations of electrons are discussed. Plasma fluxes to the wall are independent of the thermalization level except in the very-low thermalization limit, when the tail of the distribution function of bulk electrons is highly depleted. To the contrary, energy losses to the walls and the sheath charge saturation limit depend strongly on the level of thermalization. Elastically reflected electrons affect significantly the plasma response by modifying the fluxes of primary and secondary electrons at the walls. Emphasis is put on obtaining analytical expressions for main plasma magnitudes, which can be implemented in two-dimensional models of the whole plasma discharge. © *2007 American Institute of Physics*. [DOI: 10.1063/1.2749237]

I. INTRODUCTION

The plasma interaction with the lateral dielectric walls of a Hall thruster chamber leads to plasma recombination, deposition of ion and electron energy, and deposition of electron azimuthal momentum (known as "wall collisionality").[1–3] These plasma depositions affect significantly the thruster performances. In addition, ion impacts on the walls are responsible for wall erosion, which, at the end, limits the thruster lifetime. An accurate model of the plasma wall interaction is one of the main open problems in Hall thruster research. The electron velocity distribution function (EVDF) and the characteristics of the secondary electron emission (SEE) from the wall are two key aspects of this problem.

Hobbs and Wesson,[4] assuming a Maxwellian EVDF and cold SEE, showed that, as the SEE yield increases, the potential fall at the Debye sheaths around the dielectric walls decreases and the electron energy deposition increases. For a SEE yield close to 1 (~98.3% for xenon), they found that the negative (i.e., electron-repelling) sheath reaches the charge-saturation limit (CSL) and regime, which prevent the vanishing of the negative sheath and place an upper bound on the deposition of electron energy at the walls. Ahedo and co-workers applied the Hobbs-Wesson sheath model to macroscopic and hybrid two-dimensional models of the Hall thruster discharge, and found out that it yields excessive energy losses and, consequently, unreasonably strong deterioration of thruster performance.[3,5–7]

Recent works suggest that the plasma is not collisional enough to replenish the tail of high-energy electrons that impact the wall, so that the distribution function of bulk electrons is non-Maxwellian, thus presenting a smaller "effective" temperature in the direction parallel to the magnetic field.[8–13] Since the role of an electron-repelling sheath next to a dielectric wall is to balance the electron and ion fluxes, a partially depleted tail of the EVDF reduces certainly the sheath potential fall. However, the effects of a depleted tail on the ion flux itself and the energy losses, the two main magnitudes of plasma-wall interaction, need to be quantified. In addition, these magnitudes are also affected by the amount and behavior of the SEE.

Turning now to the characterization of the SEE, there are three subjects that require attention: (1) a correct secondary electron emission model; (2) the trapping and thermalization of the SEE beams within the bulk of the plasma; and (3) the magnetic effects on the SEE. Both the SEE yield and the energy distribution of emitted electrons are poorly known for the low energy range of electrons impacting with Hall thruster walls. SEE seems to be constituted by slow or "true-secondary" electrons (coming from internal layers of the wall) plus elastically and inelastically reflected electrons, with different average energies and emission yields.[14–17] At low impacting energies, elastically reflected electrons dominate, with an emission yield of about 20%–60%. The one-parameter SEE model of Hobbs-Wesson considers cold true-secondary electrons only. In a model of the full discharge, Barral *et al.*[10] took into account SEE with true-secondary electrons and a constant yield of reflected electrons with partial energy accommodation; no parametric investigation was carried out. Taccogna *et al.* have proposed a very detailed, multi (>10)-parameter SEE model.[17] Here, we will investigate the relevance of different parameters characterizing SEE, in order to propose a relative simple model that retains the main ones only. The charge saturation limit will be studied as well.

Fife[18] and Ahedo[5] assumed total thermalization of the SEE beams within the main plasma. This justified the use of a single, Maxwellian electron population in the quasineutral plasma, even for high SEE. Later, Ahedo and Parra[19] pointed

[a]Electronic mail: eduardo.ahedo@upm.es

out that weak collisionality could allow partial recollection of the SEE beams by the walls, and demonstrated that, when the recollected fraction is large, the sheaths do not reach charge-saturation and electron energy losses to the walls are much lower. Indeed the losses are similar to the zero SEE limit; i.e., about 100 times lower than for total thermalization and a charge-saturated sheath. Sydorenko *et al.*[13,20] recovered this behavior of SEE at low thermalization with a particle-based model.

Magnetic effects on true-secondary electrons have been considered partially by Sydorenko *et al.* as well. They included the effect of the $E\times B$ (azimuthal) drift imparted to beam electrons once they leave the (thin) emission sheath, and pointed out that, in the weakly collisional case, this increment of energy facilitates the partial recollection of SEE and increases the re-emission yield.

The goals of this paper are (1) to derive an quasi-analytical model of plasma-wall interaction that takes into account the combined effects of partial depletion of the main electron population and partial recollection of the SEE beams, and (2) to investigate which are the main SEE characteristics that must be retained in a SEE analytical model. Emphasis will be put on (a) comparing the low and high thermalization limits, (b) evaluating the different roles of secondary and primary electrons in the response, (c) the sensitivity of CSL conditions to different parameters, and (d) deriving simple expressions for particle and energy losses, which can be implemented in full models of the plasma discharge, such as HPHALL.[6,18] Progress on this work was presented in two conference papers.[21,22]

As in similar works, the analysis of the collisional processes determining the state of the EVDF remains out of this paper scope. The approximate expressions used for the EVDF *within the sheaths* will be based on first-principles models. Magnetic effects on the SEE will not be included in the present model. Strictly, this limits the model validity to (i) magnetic lines perpendicular to the wall and (ii) a weak enough axial (i.e., parallel to the wall) electric field E_z. Although there are uncertainties on the value of the azimuthal velocity $u_\theta \sim E_z/B$ (which is measured indirectly only), experiments and simulations would suggest that, in most Hall thrusters, $m_e u_\theta^2 \ll 3T_e$, except in a very localized zone at the center of the acceleration region, where E_z is maximum.

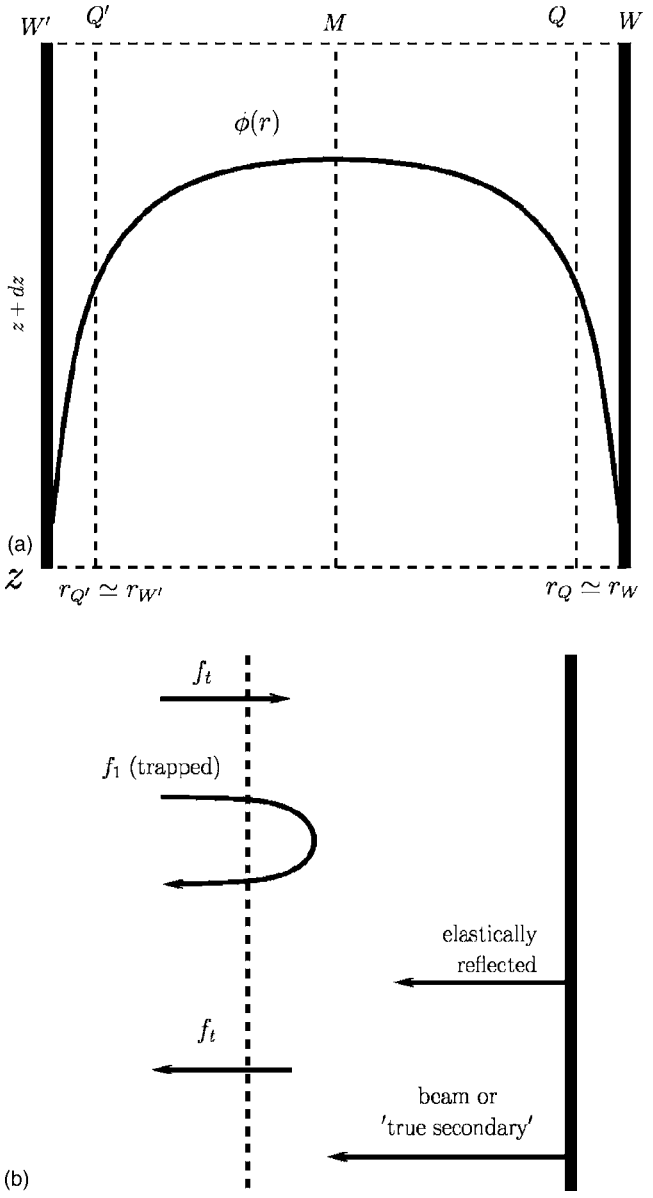

FIG. 1. (a) Sketch of the radial model with the bulk region and the two Debye sheaths. (b) Electron populations in the sheath and secondary electron emission.

II. FORMULATION OF THE ELECTRON MODEL

A stationary plasma, confined between two planar, ceramic walls is considered (Fig. 1). A one-dimensional model is proposed (which corresponds to the radial direction in a Hall thruster chamber); when necessary, axial plasma contributions are included as source terms. The zero Debye length limit is invoked, leading to a two-scale structure, consisting of the bulk region of quasineutral *plasma* and two collisionless, space-charge *sheaths* adjacent to the walls. Let point M be the channel median, points W and W′ the two walls and points Q and Q′ the edges of the two sheaths. The sheaths are semi-infinite regions in their natural scale (the Debye length) and discontinuity surfaces in the quasineutral scale (so that $r_Q=r_W=h/2$ and $r_{Q'}=r_{W'}=-h/2$). We consider only sheaths with monotonic potentials, which means that the model will not go beyond the CSL. The electric potential ϕ, instead of r, can then be used as the independent variable inside the sheath (thus avoiding to define a different spatial variable for the sheath). Let $\phi_{WQ}=\phi_Q-\phi_W$ be the potential drop in the sheath, which is part of the solution if the walls are dielectric. In order to neglect all magnetic effects in the model, we assume that the magnetic field $\boldsymbol{B}$ is radial and near uniform, and the azimuthal drift velocity u_θ is much smaller than the electron thermal velocity $c_e=\sqrt{T_e/m_e}$.

The velocity of each electron is divided into components parallel and perpendicular to $\mathbf{1}_r$, i.e., $\boldsymbol{v}=v_r\mathbf{1}_r+v_\perp\mathbf{1}_\perp$, and the electron distribution function has the functional form $f(r,v_r,v_\perp)$. The symmetry of the problem with respect to the median M implies that

$$f(r_M+\Delta r,v_r,v_\perp)=f(r_M-\Delta r,-v_r,v_\perp). \quad (1)$$

A. The electron distribution function

The EVDF $f(r,\boldsymbol{v})$ is obtained from the one-dimensional (radial) Boltzmann equation

$$v_r\frac{\partial f}{\partial r}+\frac{e}{m_e}\frac{d\phi}{dr}\frac{\partial f}{\partial v_r}=\dot{f}(r,\boldsymbol{v}), \tag{2}$$

where $\dot{f}$ accounts for collisional processes (electron-electron thermalization, electron-neutron elastic collisions, ionization), the effect of plasma instabilities, and transverse (i.e., axial) plasma diffusion (required anyway to balance the net production or loss of plasma).

In the zero Debye length limit, $\dot{f}$ can be dropped within the two thin sheaths and the EVDF depends only of the constants of motion. These consist of the parallel and perpendicular components of the electron total energy:

$$v_\perp=\text{const}, \quad m_e v_r^2/2-e\phi=\text{const}. \tag{3}$$

Therefore, the EVDF in the sheath has the functional form

$$f(\phi,v_r,v_\perp)=f_Q[v_{rQ}(\phi,v_r),v_\perp]\equiv f_W[v_{rW}(\phi,v_r),v_\perp], \tag{4}$$

where ϕ is used as independent variable,

$$v_{rQ}(\phi,v_r)=\text{sign}(v_r)\sqrt{v_r^2+2e(\phi_Q-\phi)/m_e}, \tag{5}$$

and $v_{rW}(\phi,v_r)$ satisfies a similar expression. Then, we just need to determine $f_Q(\boldsymbol{v})$ or $f_W(\boldsymbol{v})$ to know the EVDF in the sheath.

A consistent determination of the EVDF inside the sheath requires solving the Boltzmann equation in the bulk quasineutral region. Even using the simple Bhatnagar-Gross-Krook formulation[23] for $\dot{f}$, the problem faces two big difficulties: first, the quasineutrality condition implies that the potential profile $\phi(r)$ is part of the solution, and second, $\dot{f}$ depends on velocity moments of $f(r,\boldsymbol{v})$. Based on phenomenological considerations and the simple analysis carried out in Ref. 21, we assume that the distribution function at the sheath edge Q can be expressed as

$$f_Q(v_r,v_\perp)=\begin{cases} f_{fQ}(v_r,v_\perp), & v_r<-v_{WQ},\\ f_1(v), & |v_r|<v_{WQ},\\ f_{tQ}(v_r,v_\perp), & v_r>v_{WQ}, \end{cases} \tag{6}$$

where $v_{WQ}=\sqrt{2e\phi_{WQ}/m_i}$, f_{tQ} corresponds to electrons impinging into the wall W, f_{fQ} corresponds to electrons emitted or reflected at wall W, and f_1 corresponds to the population of primary (or bulk or thermalized) electrons. The population f_f of electrons *from* the wall depends on the SEE properties of wall W and will be discussed below. A Maxwellian function is used to define the primary population,

$$f_1(v)=n_1\left(\frac{m_e}{2\pi T_1}\right)^{3/2}\exp\left(-\frac{m_e v^2}{2T_1}\right), \tag{7}$$

where n_1 and T_1 are constants (notice that the actual distribution function of primary electrons is determined below). The population f_t at Q of electrons going *to* the wall satisfies

$$f_{tQ}(v_r,v_\perp)=(1-\sigma)f_{fQ'}(v_r,v_\perp)+\sigma f_1(v), \tag{8}$$

where the first term on the right-hand side is the nonthermalized fraction at Q of electrons coming from wall W′, the second term corresponds to primary electrons, and

$$\sigma(\boldsymbol{v})=1-\exp[-h/\lambda_{\text{ther}}(\boldsymbol{v})] \tag{9}$$

is the function representing the thermalization fraction, which depends on the thermalization mean-free-path $\lambda_{\text{ther}}(\boldsymbol{v})$, and the channel width h. In the absence of a reliable model for the electron thermalization, we take $\sigma(\boldsymbol{v})=\text{const}$, as in Ref. 13.

Secondary electron emission at wall W depends on the distribution of electrons impacting the wall,

$$f_{tW}(v_r,v_\perp)=\sigma e^{-\hat{\phi}_{WQ}}f_1(v)H(v_r)+(1-\sigma)f_{fW'}(v_r,v_\perp); \tag{10}$$

here, Eqs. (4) and (8) have been used, $\hat{\phi}_{WQ}=e\phi_{WQ}/T_1$, and $H(v_r)$ is the Heaviside step function. For the purposes of the present work, only the main aspects of the experimental data on SEE are modeled. Thus, the SEE yield is assumed to have contributions of elastically reflected electrons and true-secondary or beam electrons,

$$\delta_s(E)=\delta_{sb}(E)+\delta_{sr}(E), \tag{11}$$

with $E=mv^2/2$ the energy of the impacting electron. Subscripts r and b stand for "reflected" and "beam," respectively, with the last name justified on their emission energy ($\sim$1–3 eV) being generally much less than the sheath potential fall and the temperature of primary electrons ($\sim$5–50 eV). Based on experimental data[14,15,24,25] and previous models,[10,17,26] the partial SEE yields are assumed to follow the simple linear laws

$$\delta_{sb}=E/E_b, \quad \delta_{sr}=\delta_0\exp(-E/E_r); \tag{12}$$

in particular, the exponentially decaying law for $\delta_{sr}(E)$ is suggested by results from Refs. 14, 15, and 17. A constant value for δ_{sr} was used by Barral *et al.*[10] A possible small threshold energy (of a few eV) in δ_{sb} has been neglected because of its small impact on the response. Typical values for boron nitride ceramics, used in Hall thrusters, would be $E_r\sim E_b\sim 50$ eV, $\delta_0\sim 0.4$–0.6, and $E_b\sim 40$ eV. Notice that the crossover energy E_1 for the total SEE yield comes out from

$$E_1=[1-\delta_{sr}(E_1)]E_b. \tag{13}$$

The distribution of electrons from wall W is modeled as

$$f_{fW}(v_r,v_\perp)=\delta_{sr}(E)f_{tW}(-v_r,v_\perp)+f_2(v)H(-v_r), \tag{14}$$

where the first term on the right-hand side corresponds to reflected electrons and

$$f_2(v)=g_2\sqrt{\frac{2\pi m_e}{T_2}}\left(\frac{m_e}{2\pi T_2}\right)^{3/2}\exp\left(-\frac{m_e v^2}{2T_2}\right) \tag{15}$$

models the distribution of emitted beam electrons, with

$$g_2 = \int d^3v v_r \delta_{sb}(E)[1-\delta_{sr}(E)] f_{t\mathrm{W}}(v_r, v_\perp) \tag{16}$$

representing their particle flux. Obviously, only electrons collected by the wall can produce true-secondary emission. The emission temperature T_2 ($\sim$1–3 eV) is the fourth parameter of the SEE model, and, as commented before, T_2/T_1 is small in most of (or all) the thruster chamber.

The populations of electrons to and from the wall [Eqs. (10) and (14)] can now be expressed as linear combinations of distributions f_1 and f_2,

$$f_{t\mathrm{W}}(v_r, v_\perp) = [\sigma \mathrm{e}^{-\hat{\phi}_{\mathrm{WQ}}} f_1(v) + (1-\sigma) f_2(v)] \kappa H(v_r), \tag{17}$$

$$f_{f\mathrm{W}}(v_r, v_\perp) = [\delta_{sr} \sigma \mathrm{e}^{-\hat{\phi}_{\mathrm{WQ}}} f_1(v) + f_2(v)] \kappa H(-v_r). \tag{18}$$

Here,

$$\kappa(\delta_{sr}, \sigma) = \frac{1}{1-(1-\sigma)\delta_{sr}} \tag{19}$$

is a gain factor representing the cumulative effect of the subsequent reflections of electrons with the walls. The two contributions to $f_{t\mathrm{W}}$ in Eq. (17) are the replenished tail of primary electrons and the nonthermalized beam electrons. Since one has $\sigma\kappa < 1$ for $\sigma < 1$ and $\forall \delta_{sr}$, partial thermalization always implies a partial depletion of the incident tail of primary electrons. On the contrary, $(1-\sigma)\kappa$ can be larger than 1 (in particular, for $\sigma \ll 1$ and $\delta_{sr} > 0$).

We can now express the electron distribution function at any location inside the sheath (defined by its local potential ϕ) as the sum of the contributions of the distributions of primary and beam electrons,

$$f(\phi, \boldsymbol{v}) = f_p(\phi, \boldsymbol{v}) + f_b(\phi, \boldsymbol{v}), \tag{20}$$

with

$$f_p(\phi, v_r, v_\perp) = f_1(v) \mathrm{e}^{e(\phi-\phi_{\mathrm{Q}})/T_1} \begin{cases} \delta_{sr}\sigma\kappa, & v_r < -v_{r0}, \\ 1, & |v_r| < v_{r0}, \\ \sigma\kappa, & v_r > v_{r0}, \end{cases} \tag{21}$$

$$f_b(\phi, v_r, v_\perp) = f_2(v) \mathrm{e}^{e(\phi-\phi_{\mathrm{W}})/T_2} \begin{cases} \kappa, & v_r < -v_{r0}, \\ 0, & |v_r| < v_{r0}, \\ (1-\sigma)\kappa, & v_r > v_{r0}, \end{cases} \tag{22}$$

where $v_{r0} = \sqrt{2e(\phi-\phi_{\mathrm{W}})/m_e}$.

B. Fluxes of particles and energy

The fluxes of particles and energy at the wall satisfy

$$g_e = \int d^3v v_r f_{\mathrm{W}}(v_r, v_\perp), \tag{23}$$

$$q_{e\mathrm{W}} = \int d^3v v_r \frac{1}{2} m v^2 f_{\mathrm{W}}(v_r, v_\perp). \tag{24}$$

Notice that particle fluxes are constant across the sheath but energy fluxes are not; at the sheath edge, $q_{e\mathrm{Q}} = q_{e\mathrm{W}} + \phi_{\mathrm{WQ}} g_e$.

Because of the presence of δ_{sr} in function κ, the above integrals cannot be expressed in a simple nonintegral form except for $\delta_{sr}(E) = \mathrm{const}$ (i.e., $E_r = \infty$) or $\sigma = 1$. We solve next the problem for $\delta_{sr} = \mathrm{const}$ and postpone the more general case to Sec. IV B. Using Eqs. (17) and (18), one has

$$g_e = g_p - g_b, \quad q_{e\mathrm{W}} = 2T_1 g_p - 2T_2 g_b, \tag{25}$$

with

$$g_p = (1-\delta_{sr})\sigma\kappa \mathrm{e}^{-\hat{\phi}_{\mathrm{WQ}}} n_1 \sqrt{T_1/2\pi m_e}, \quad g_b = \sigma\kappa g_2, \tag{26}$$

the *net* fluxes or primary and beam electrons, respectively. Notice that g_2 [Eq. (16)] is only the flux of "new" beam electrons; g_2 and g_b coincide only for total thermalization ($\sigma = 1$).

For $\delta_{sb}(E)$ linear, this flux of emitted beam electrons satisfies

$$g_2 = (1-\delta_{sr}) q_{t\mathrm{W}}/E_b, \tag{27}$$

where

$$q_{t\mathrm{W}} = \frac{g_p}{1-\delta_{sr}} \frac{2T_1}{E_b} + \kappa(1-\sigma)\frac{2T_2}{E_b} g_2 \tag{28}$$

is the energy flux incident into the wall. Solving Eq. (27) for g_2, the net beam (or true-secondary) yield (defined as the ratio between beam and primary net fluxes) is

$$\frac{g_b}{g_p} \equiv \gamma_{bp} = \sigma\kappa\gamma_{2p}, \quad \gamma_{2p} = \frac{2T_1}{E_b - \kappa(1-\sigma)(1-\delta_{sr})2T_2}, \tag{29}$$

where $\gamma_{2p} \equiv g_2/g_p$ is the average emission yield of true-secondary electrons.

The Appendix gives expressions for other magnitudes of interest, such as the partial densities of primary and beam electrons, n_p and n_b, respectively, and the temperature $T_{rp\mathrm{Q}}$ of primary electrons in the direction parallel to the magnetic field (it is immediate that the perpendicular temperature of primary electrons is T_1).

III. CLOSURE OF THE SHEATH MODEL

The parameters involved in the EVDF model can be divided in several groups. The first one consists of the type of gas (which defines the ratio $\sqrt{m_i/m_e}$) and the reference values n_1 and T_1. These are used to define nondimensional variables

$$\hat{n} = \frac{n}{n_1}, \quad \hat{g} = \frac{g}{n_1\sqrt{T_1/m_i}}, \quad \hat{T} = \frac{T}{T_1}, \quad \hat{\phi} = \frac{e\phi}{T_1}, \tag{30}$$

and so on. The second group consists of the thermalization factor σ and the four parameters of the SEE model: T_2, E_b, E_r, and δ_0. Finally, there is the sheath potential fall ϕ_{WQ}.

If the potential fall is known (for a conducting wall, for instance) the model of Sec. II would be complete in order to determine the EVDF and the electron-wall interaction. Figures 2(a) and 2(b) plot an example of the evolution of the EVDF inside a sheath, with ϕ acting as spatial variable. Figure 2(b) compares the EVDF at the two sheath ends; beam electrons and the partially depleted tail of primary electrons are clearly observable in f_{Q}. Figure 2(c) has illustrative pur-

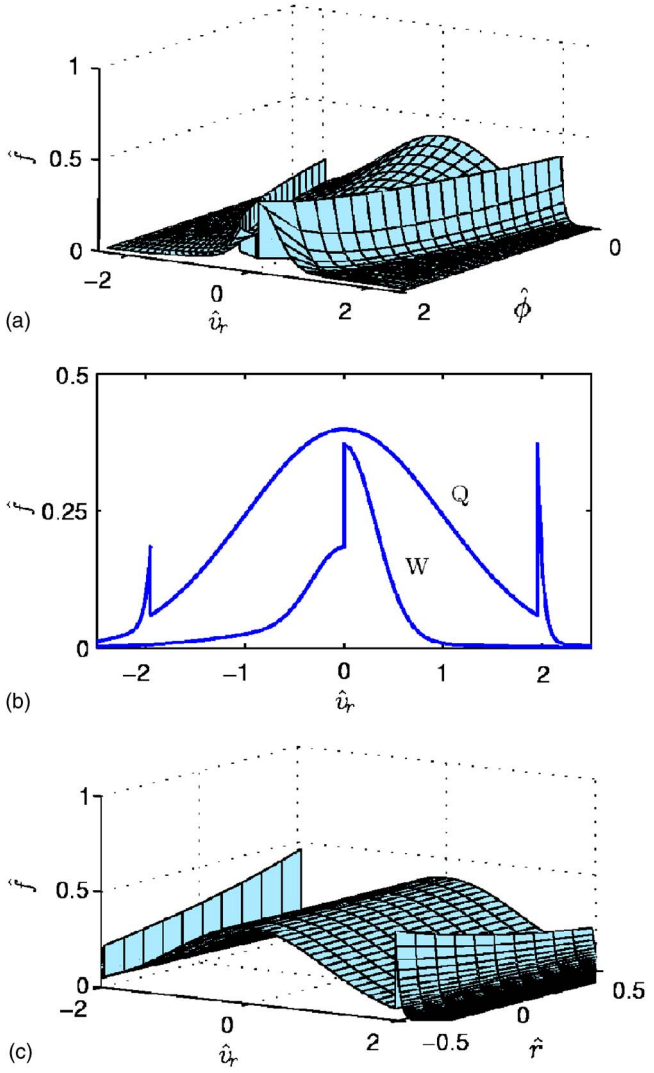

FIG. 2. (Color online) (a) Evolution of the distribution function in the sheaths for $\sigma=0.6$, $T_2/T_1=0.1$, $\delta_{sr}=0.25$, $E_b/T_1=1.5$, and $\hat{\phi}_{WQ}=1.91$. Dimensionless variables are $\hat{r}=r/h$, $\hat{v}=v_r\sqrt{m_e/T_1}$, and $\hat{f}(r,v_r)=n_1^{-1}\sqrt{T_1/m_e}\int_0^\infty dv_\perp 2\pi v_\perp f(r,v_r,v_\perp)$. Regions $v_r<0$ and $v_r>0$ correspond to distributions f_f and f_t, respectively, of electrons from wall and to wall. (b) Comparison of the EVDF at the two sheath ends, Q and W. (c) Illustration of the evolution of the distribution function in the bulk region (for ϕ=const).

poses only: it shows the profiles of the EVDF in the bulk of the plasma for constant electric potential there. Observe the two counterstreaming beams of secondary electrons and their partial thermalization.

For dielectric walls, the potential fall $\hat{\phi}_{WQ}$ is determined from the condition of zero electric current at the wall,

$$g_e = g_i \equiv j_{iW}/e, \tag{31}$$

with j_{iW} the ion density current into sheath and wall. This condition couples the ion and electron problems. Since j_{iW} is going to depend only weakly on σ and the SEE model, it is convenient to rewrite the expressions of Eq. (25) in the form

$$g_p = \frac{g_i}{1-\gamma_{bp}}, \quad q_{eW} = \frac{2T_1 - 2T_2\gamma_{bp}}{1-\gamma_{bp}} g_i. \tag{32}$$

Substituting g_p in the first equation with Eq. (26) and solving for the sheath potential, one has

$$\exp \hat{\phi}_{WQ} = \sqrt{\frac{m_i}{2\pi m_e}} \times \frac{\sigma\kappa}{\hat{g}_i} \times (1-\delta_{sr})(1-\gamma_{bp}). \tag{33}$$

The ion current into the sheath depends on the plasma behavior in the bulk region. As an example and in order to close the model, we determine next j_{iW} for the simplest case of a stationary regime and singly-charged, quasicold ions.

A. A simple ion model

In a stationary regime, the ion current into the sheath is determined self-consistently from the Bohm condition at the sheath edge. The Poisson equation for the sheath potential is

$$\frac{d^2\phi}{dr^2} = \frac{e}{\epsilon_0}[n_e(\phi) - n_i(\phi)], \tag{34}$$

where the ion and electron densities depend only on ϕ. It is well known that the development of a space-charge, monotonic solution from point Q^+ (on the sheath side) requires to satisfy the generic Bohm condition

$$\frac{d}{d\phi}[n_e(\phi) - n_i(\phi)]_{Q^+} \geq 0. \tag{35}$$

Furthermore, if the response is stationary in the quasineutral region, only the marginal (or sonic) form of the Bohm condition applies.

The density of a quasicold, singly charged ion population satisfies

$$n_i(\phi) = g_i[(g_i/n_{eQ})^2 + 2e(\phi_Q - \phi)/m_i]^{-1/2}, \tag{36}$$

where quasineutrality at Q has been applied. The marginal case of Eq. (35) then leads to

$$g_i = n_{eQ}u_{riQ}, \quad u_{riQ} = \sqrt{\left.\frac{en_{eQ}}{m_i}\frac{d\phi}{dn_e}\right|_{Q^+}}, \tag{37}$$

which is further developed in Eq. (A3) of the Appendix. This expression states that, for a cold ion population, g_i depends only on the electron density around Q. For the simple case of zero SEE and a nondepleted Maxwellian distribution, the Bohm condition states that ions enter the sheath with the sound velocity $\sqrt{T_1/m_i}$.

B. The charge saturation limit

The above plasma model assumes that the electric field is monotonic in each half-channel. This condition is no longer valid when the electric field in the sheath becomes zero at the wall boundary, i.e., $d\phi/dr|_W=0$, which is known at the charge saturation limit.[4] The integration the Poisson equation across the sheath shows that the condition $d\phi/dr|_W \leq 0$ is equivalent to

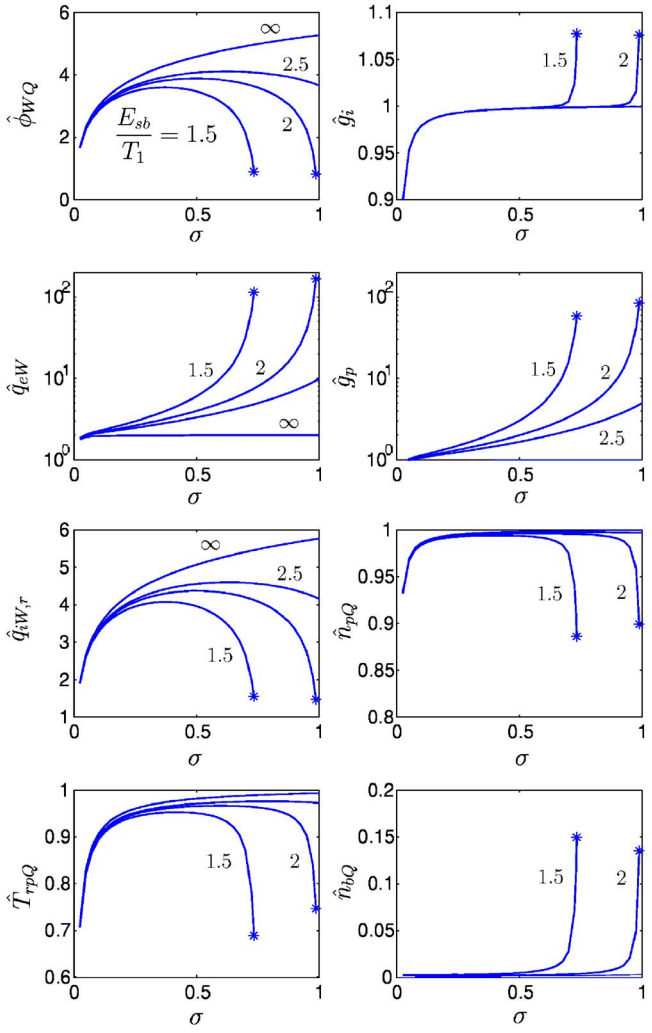

FIG. 3. (Color online) Influence on the plasma-wall response of the electron thermalization level and SEE crossover energy for $E_b/T_1=1.5$, 2, 2.5, and ∞, $T_2/T_1=0.01$, and $\delta_{sr}=0$ (thus $E_1=E_b$). Asterisks correspond to the CSL. This and following figures are for xenon ($\sqrt{m_i/m_e}\simeq 490$).

$$\int_{\phi_W}^{\phi_Q} e(n_i-n_e)d\phi \geq 0; \tag{38}$$

that is, the net electric charge inside a monotonic sheath is non-negative. This equation, detailed in the Appendix, will be used to determine the CSL. The plasma response beyond the CSL[16] is not considered in this paper.

IV. RESULTS

The main magnitudes of plasma-wall interaction affecting Hall thruster performances are: (i) the plasma flux to the wall, i.e., g_i $(=g_e)$ [Eq. (32)], which is recombined and requires to be reionized; (ii) the deposition of electron energy, q_{eW}, which is the main source of plasma-cooling and wall-heating; and (iii) the ion energy flux into the wall,

$$q_{iW}=(m_i u_{iQ}^2/2+e\phi_{WQ})g_i, \tag{39}$$

which, apart from producing additional wall heating, is the responsible for wall sputtering. The present radial model gives information only on the flux of radial ion energy $q_{iW,r}=(m_i u_{riQ}^2/2+e\phi_{WQ})g_i$.

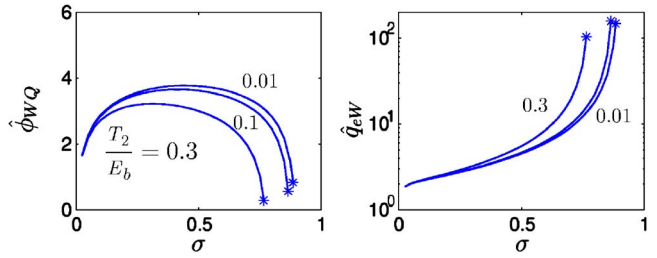

FIG. 4. (Color online) SEE model. Effect of the emission energy of "true-secondary" electrons: $T_2/E_b=0.01$, 0.1, and 0.3; $E_b/T_1=1.8$ and $\delta_{sr}=0$. Asterisks correspond to the CSL.

A. Influence of the thermalization level

Figure 3 depicts, for the simplest SEE model ($\delta_{sr}=0$ and $T_2/T_1\ll 1$), the combined influence of the electron thermalization level σ and SEE crossover energy E_1 $(=E_b)$, on the main plasma-wall variables. Both parameters affect strongly the plasma response. The plasma flux $\hat{g}_i$, governed by Bohm condition, remains close to 1 always (except for $\sigma\to 0$). The sheath potential fall $\hat{\phi}_{WQ}(\sigma)$ presents a maximum for an intermediate thermalization level. This behavior of $\hat{\phi}_{WQ}$ is easy to understand from Eq. (33): The first factor in the right-hand side of Eq. (33) is large ($\sim$200 for xenon), the second one is the effect of partial thermalization on the primary electron population, and the last one is the contribution of secondary, beam electrons. Therefore, for any of the last two factors to affect the value of ϕ_{WQ} significantly, they must be small. This occurs for either $\sigma\ll 1$, i.e., the low-thermalization limit, or $1-\gamma_{bp}\ll 1$, which corresponds to the vicinity of the charge-saturation limit. The density of beam electrons n_b at the sheath edge (and in the bulk region) is negligible. A partial exception is at the CSL, where $\hat{n}_{bQ}$ is the responsible for the increment of $\hat{g}_i$ above 1.

The most dramatic dependence with σ corresponds to the deposition of electron energy q_{eW}, which increases from $q_{eW}/2T_1g_i\simeq 1$ at $\sigma\ll 1$ to $q_{eW}/2T_1g_i\simeq 100$ at the CSL. This increment is due to the increase of the flux of primary electrons g_p [Eq. (32)]. The evolution of $q_{iW,r}(\sigma)$ follows that of ϕ_{WQ}, with a maximum at an intermediate thermalization level (which can lead to maximum wall sputtering there).

In our first approach to this model,[21] we assumed a constant-frequency model (i.e., $\lambda_{ther}/v_{re}=$const) instead of a constant-mean-free-path one. It can be checked now that both models lead to the same trends in the solution, but the present model yields much simpler expressions.

B. Influence of the emission model

Figure 4 shows the effect of a finite temperature of true-secondary electrons; i.e., T_2. The increase of T_2/E_b yields a larger δ_{sb} and thus a larger γ_{bp}. This leads to larger g_p and q_{eW}, and lower ϕ_{WQ}. The exception is $\sigma\simeq 1$, when the only effect of increasing T_2 is to reduce q_{eW}. The parameter T_2/E_b is always small and we expect solutions for $T_2/E_b\simeq 0$ to

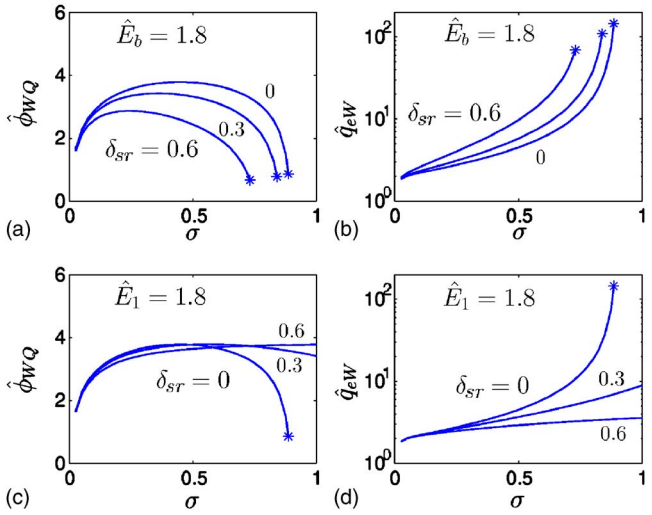

FIG. 5. (Color online) SEE model. Effect of the presence of elastically reflected electrons: δ_{sr}=0, 0.3, and 0.6; T_2/T_1=0.01; and E_b/T_1=1.8 in (a)–(b), E_1/T_1=1.8 in (c)–(d). Asterisks correspond to the CSL.

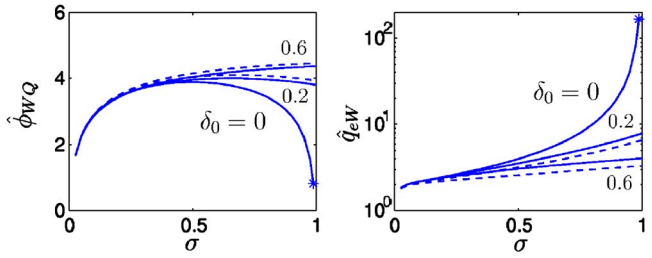

FIG. 6. (Color online) SEE model. Effect of $\delta_{sr}(E)=\delta_0 \exp(-E/E_r)$ for δ_0 =0, 0.2, and 0.6, E_r/T_1=2, $(1-\delta_0)E_b/T_1$=2, and T_2/T_1=0.01. Dashed lines correspond to use the approximate function $\tilde{\delta}_{sr}(T_1)$ of Eq. (40). Asterisks correspond to the CSL.

yield errors of order $O(T_2/E_b)$. In Sec. VI we show that this is no longer true for the CSL, where errors are of order $O(\sqrt{T_2/E_b})$.

The presence of elastically reflected electrons modifies the sheath parameters more deeply, since these electrons are hot. Figures 5(a)–5(d) show the effect of a SEE yield with a 0%–60% fraction of elastically reflected electrons. Notice that the plots differ on the SEE energy that is kept constant: $\hat{E}_b$ in Figs. 5(a) and 5(b) and $\hat{E}_1=(1-\delta_{sr})\hat{E}_b$ in Figs. 5(c) and 5(d). The different plasma behavior is due to $\partial\gamma_{bp}/\partial\delta_{sr}$ being positive for $\hat{E}_b$=const, and negative for $\hat{E}_1$=const. This illustrates that in order to understand correctly the plasma response we must interpret first the role and relevance of the several plasma conditions and parameters. The analysis shows that the zero-electric-current and Bohm conditions are the two affecting the most the plasma response. Since g_i varies weakly, the key parameter (for T_2/E_b small) is the relative beam-to-primary net electron flux, $\gamma_{bp}\equiv g_p/g_b$, which, through Eq. (32), self-determines the primary flux g_p and therefore the energy losses q_{eW}. The sheath potential fall [Eq. (33)], is then self-adjusted in order the wall collects the appropriate flux of primary electrons.

Up to here we have assumed $\delta_{sr}(E)$=const in order to obtain simple relationships among the parameters that facilitate their interpretation. There is no difficulty in obtaining results with E_r finite in Eq. (12): expressions for the fluxes just keep their integral form. Figure 6 plots some solutions with E_r finite. As expected, there are no qualitative changes with respect to the case δ_{sr}=const. This leads us to propose an approximate emission model that keeps the dependence of δ_{sr} on the energy of impacting electrons but profit simultaneously from the simple expressions of Secs. II and III. The idea is to substitute the "exact" yield $\delta_{sr}(E)$ by an "average" one, $\tilde{\delta}_{sr}$, which depends directly on the main electron temperature T_1. A satisfactory enough agreement is reached using the approximate SEE yield

$$\tilde{\delta}_{sr}(T_1) = \delta_0 \frac{E_r^2}{(E_r + T_1)^2} \tag{40}$$

in the analytical expressions of Secs. II and III. The dashed lines of Fig. 6 correspond to this approximate model.

V. THE LOW-THERMALIZATION LIMITS

For total thermalization, the present model recovers the results of Ref. 5. The case of low thermalization is of special interest here because (i) it presents important differences with total thermalization, (ii) it admits some asymptotic expressions, and (iii) it could be the appropriate one for Hall thruster discharges (a value of $\sigma\sim 1\%$ is suggested in Ref. 20, which, for T_1=30 eV and a chamber width of 15 mm, corresponds to a thermalization frequency of $\sim 2.4\times 10^6$ s^{-1}).

Let us analyze now how low thermalization of beam and primary electrons affect in different ways the plasma response. For $\sigma \ll 1$, the effective secondary yields are

$$\gamma_{bp} \simeq \frac{\sigma}{1-\delta_{sr}}\gamma_{2p}, \quad \gamma_{2p} \simeq \frac{2T_1}{E_b - 2T_2}. \tag{41}$$

Therefore, independent of the emission of beam electrons (γ_{2p}) being small or large, low thermalization makes the two counter-streaming SEE beams of almost equal current and leads to a very small value of the effective beam-to-primary flux ratio γ_{bp}.[19] The consequences are $g_p \simeq g_i$ and $q_{eW} \simeq 2T_1 g_i$; that is, energy losses are at their minimum. On the other hand, the sheath potential fall satisfies

$$\hat{\phi}_{WQ} \simeq \ln\left(\frac{\sigma}{\hat{g}_i}\sqrt{\frac{m_i}{2\pi m_e}}\right). \tag{42}$$

Here, the factor σ is measuring the depletion of the tail of primary electrons impinging the wall; $\sigma \ll 1$ indicates that a lower $\hat{\phi}_{WQ}$ is needed to adjust the electron flux to the ion flux. In addition, $\gamma_{bp} \ll 1$ makes that SEE beams do not affect the sheath potential fall.

The behavior of $\hat{\phi}_{WQ}$ for very low thermalization is not immediate since Eq. (A3) indicates that $\hat{g}_i \to 0$ goes to zero when $\hat{\phi}_{WQ} \to 0$. From Eqs. (33) and (A1)–(A3), the asymptotic plasma behavior for the "very-low thermalization limit" (VLTL),

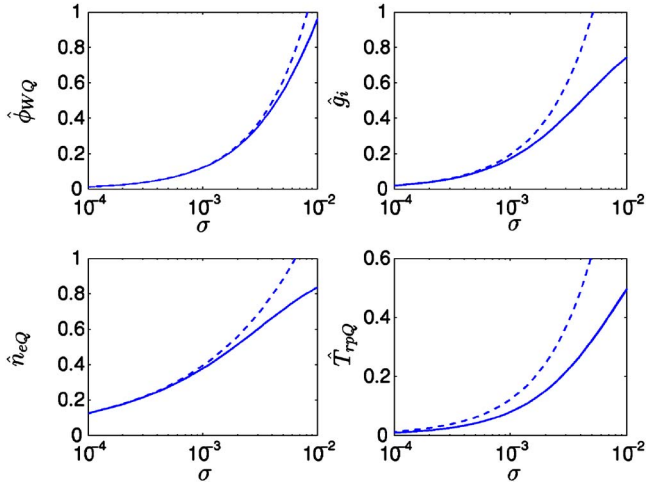

FIG. 7. (Color online) Low thermalization limit. Same cases as in Fig. 3. Dashed lines correspond to the very-low thermalization limit [Eq. (44)].

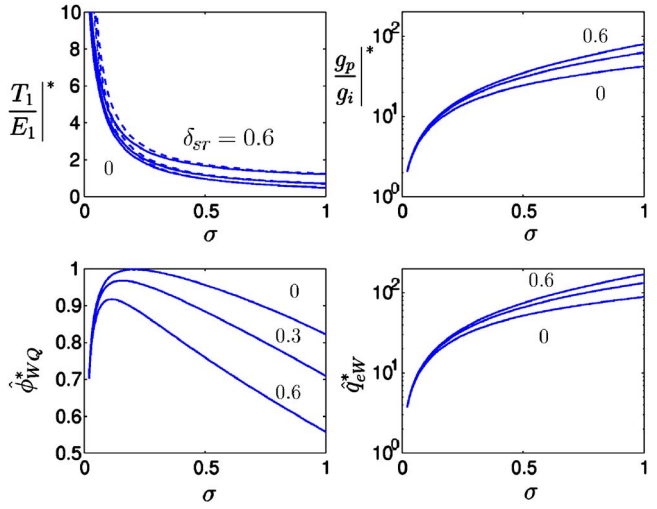

FIG. 8. (Color online) Charge saturation limit. Variation of main parameters with σ for $\delta_{sr}=0$, 0.3, 0.6; other parameters: $T_2/T_1=0.1$. Dashed lines for T_1^* correspond to Eq. (46).

$$\sigma' = \sigma(m_i/m_e)^{1/2} \ll 1, \tag{43}$$

is

$$\hat{g}_i \simeq \frac{\sigma'}{\sqrt{2\pi}}, \quad \hat{\phi}_{\mathrm{WQ}} \simeq \frac{\sigma'}{4}, \quad \hat{n}_{e\mathrm{Q}} \simeq \hat{n}_{p\mathrm{Q}} \simeq \sqrt{\frac{\sigma'}{2}},$$
$$\hat{T}_{rp\mathrm{Q}} \simeq \frac{\sigma'}{6}. \tag{44}$$

Figure 7 shows the evolution of these parameters in the low and very-low σ ranges. Notice that as long as $\sigma \geq O(\sqrt{m_e/m_i}) \sim 2\times 10^{-3}$, the order of magnitude of the main plasma parameters remains unchanged. Only in the VLTL, one can say that there is a strong depletion of the EVDF, leading to $T_{rp\mathrm{Q}}/T_1$ clearly below 1. It is interesting to observe that, for the VLTL, the ion velocity at the entrance of the sheath satisfies

$$m_i u_{ri\mathrm{Q}}^2 \simeq 3T_{rp\mathrm{Q}}. \tag{45}$$

Therefore, at the VLTL, the Bohm condition is preserved but the relevant temperature is the parallel to the magnetic field. The factor of 3 is due to the strong distortion of the EVDF shape from a Maxwellian one and would indicate a one-dimensional adiabatic behavior.

VI. THE CHARGE SATURATION LIMIT

This limit is the transition to a nonmonotonic structure of the Debye sheath.[16] Its importance here lies in that it sets a local minimum of the sheath potential fall and a maximum of deposition of (dimensionless) electron energy. The CSL is defined by condition (A4). The numerical computations confirm that, in order to reach the CSL, the flux of primary electrons must be much larger than the ion flux (i.e., $g_p/g_i \gg 1$), which means that the beam and primary fluxes are very similar; that is, $\gamma_{bp} \simeq 1$ in Eq. (32). The ratio g_p/g_i is plotted in Fig. 8, together with main plasma magnitudes at the CSL; an asterisk is used as superscript for parameters at the CSL.

The temperature of primary electrons (T_1) leading to sheath charge-saturation can be obtained from the approximation $\gamma_{bp}=1$. Solving this equation for T_1 and using Eqs. (13) and (40), one has

$$2\frac{T_1^*}{E_1} \simeq \frac{1}{\sigma} + \frac{\tilde{\delta}_{sr}^*}{1-\tilde{\delta}_{sr}^*} - \frac{(1-\sigma)(1-\tilde{\delta}_{sr}^*)}{\sigma} 2\frac{T_2}{E_1}, \tag{46}$$

with $\tilde{\delta}_{sr}^* = \tilde{\delta}_{sr}(T_1^*)$. This expression is explicit for T_1^* only if the yield for backscattered electrons $\tilde{\delta}_{sr}$ is constant. Figure 8 and Eq. (46) show that the plasma temperature T_1^* required to reach the CSL decreases as: (a) electron thermalization in the bulk of the plasma (i.e., σ) increases; (b) the average SEE yield is higher (i.e., E_b is lower); or (c) the "average" temperature of the SEE increases (i.e., either δ_{sr} or T_2 increase). For typical values of E_b, T_2, and T_1 in Hall thrusters, the CSL is unattainable for low thermalization [say, for $\delta_{sr} \geq 0.3$ and $\sigma \leq 0.20$ (i.e., $\lambda_{\mathrm{ther}}/h > 4.5$)]. A second positive aspect of low thermalization and CSL is that energy losses are typically one order of magnitude less than for total thermalization. The CSL behavior obtained here is the same obtained in Ref. 19 (for $\delta_{sr}=0$) except for the value of the potential fall, $\hat{\phi}_{\mathrm{WQ}}^*$, which was larger there since the depletion of primary population was not taken into account.

The approximation $\gamma_{bp}=1$ cannot be used, of course, to compute the large values of parameters $(g_p/g_i)^*$ and $(q_{e\mathrm{W}}/2T_1 g_i)^*$ [Eq. (32)], and the potential fall at the CSL $\hat{\phi}_{\mathrm{WQ}}^*$ [Eq. (32)]. The importance of computing exactly enough the ratio $(g_p/g_i)^*$ is illustrated in Table I, which compares the results of the Hobbs-Wesson model with ours. The case treated by these authors corresponds to $\sigma=1$, $\delta_{sr}=0$, and $T_2/T_1=0$, *except that* they computed the density of primary electrons (n_p) using the complete Maxwellian distribution (including the empty tail of electrons collected by the wall). This inconsistency would not be important if the potential fall at the CSL was large, but Table I shows that it leads to errors of 20% on $(g_p/g_i)^*$ and the deposition of electron energy. The influence of the temperature T_2 of beam electrons

TABLE I. CSL parameters. "FM" stands for the full-Maxwellian distribution assumed by Hobbs and Wesson; "CM" stands for the corrected Maxwellian with the empty tail of collected electrons. Other parameters: $\sigma=1$ and $\delta_{sr}=0$.

	$(g_p/g_i)^*$	$(q_{eW}/2T_1g_i)^*$	$\hat{\phi}^*_{WQ}$	$\hat{g}^*_i$
FM, $\hat{T}_2=0$	59.7	59.7	1.02	1.08
CM, $\hat{T}_2=0$	74.1	74.1	0.91	1.03
CM, $\hat{T}_2=0.01$	79.8	79.0	0.82	1.04
CM, $\hat{T}_2=0.1$	94.5	85.1	0.63	1.06

on $(g_p/g_i)^*$ is also worth commenting on. In most of the Hall thruster chamber, the ratio T_2/T_1 is of the order of 0.1, which makes it plausible to treat the "beam-secondary" population as cold[4,5] (except in the very vicinity of the wall). Errors on energy deposition and sheath potential fall are expected to be of order T_2/T_1. This turns out to be true *except for* the CSL, when they are of order $\sqrt{T_2/T_1}$, as Eq. (A6) explains and Table I illustrates. Therefore, "small" contributions (or details) of the electron model have a significant effect on the plasma parameters at the CSL.

VII. A PRACTICAL EXAMPLE AND ADDITIONAL CONSIDERATIONS

Figures 3–8 have presented dimensionless curves that allow to evaluate the relevance of the different aspects of the model. In order to complete the illustration of the influence of partial thermalization on the plasma-wall interaction, Fig. 9 presents dimensional results for typical plasma values of a conventional stationary plasma thruster (SPT) of the 1–2 kW range[27] and lateral walls made of boron nitride; the SEE data for this material have been taken from Ref. 17. A crossover energy E_1 of 40 eV is taken, and solid and dashed lines differ on the contributions of true-secondary and elastically reflected electrons. Thermalization levels from $\sigma=0.01$ to $\sigma=1$ are considered; for a chamber width of $h=15$ mm and electron energies of 50 eV, the range $\sigma=10^{-2}-10^{-1}$ corresponds to mean free paths of 0.14–1.4 m and thermalization frequencies of $2\times10^6-2\times10^7$ s^{-1}. Figure 9 plots the sheath potential fall, the ion/electron current to the wall, and the electron energy deposited at the wall; ion energy losses follow the trends of the sheath potential fall. Notice that particle and energy fluxes to the wall are proportional to the plasma density at the sheath edge, i.e., n_{eQ} (which is about a 50%–60% of the electron density at the channel median). The plots shows that the thermalization level is very crucial when estimating plasma-wall parameters. In particular electron energy losses can vary by two orders of magnitude, but for the range of temperatures of interest, the large electron energy losses at the charge-saturation regime (CSR) are attained only if the thermalization level is high. On the other hand, the presence of a significant fraction of "hot" backscattered electrons (i.e., dashed lines) has a secondary effect, except for the retardation of the CSL at high thermalization. These are positive news for modelling since the uncertainties on the distribution function of secondary electrons are large. The values of ion current to the wall in Fig. 9 are of the order of those measured by Kim *et al.*[27] As explained before, the ion current into sheath and wall depends mainly on the plasma physics in the bulk region, and is weakly affected by the thermalization level and the SEE details. The reduction of the ion current for $\sigma=0.01$ is due to the decrease of the effective parallel temperature of primary electrons; the increase of the ion current for $\sigma=1$ at the CSR is the effect of an increase of the secondary beam density (see $\hat{n}_{bQ}$ in Fig. 3).

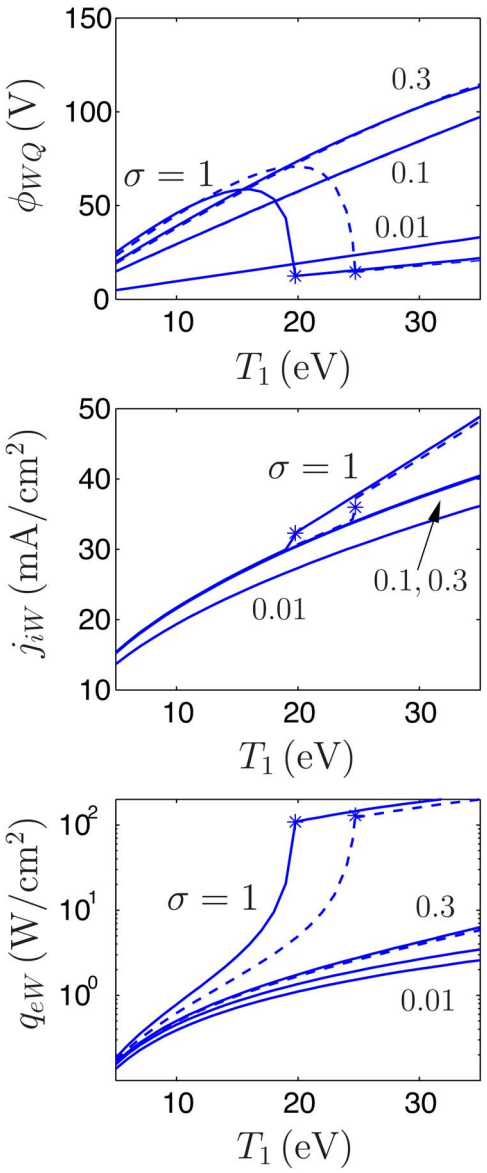

FIG. 9. (Color online) Sheath potential fall, ion current to wall, and electron energy deposition at walls, versus the perpendicular temperature of primary electrons T_1 for: different thermalization levels ($\sigma_1=0.01$, 0.1, 0.3, and 1); $n_{eQ}=5\times10^{17}$ m^{-3}; $E_1=40$ eV; $T_2=2$ eV; and $\delta_{sr}=0$ (solid lines), $\delta_0=0.45$ and $E_r=50$ eV (dashed lines). The regions to the right of the asterisk of the curves of $\sigma=1$ correspond (approximately) to the charge-saturation regime.

The curves for $\sigma=1$ and $\delta_{sr}=0$ in Fig. 9 correspond to the model presented in Ref. 5 which is currently implemented in the simulation code HPHALL-2 of the plasma discharge.[6] There are no difficulties on implementing the five-parameter SEE model proposed here in the simulation

code, but we can predict that changes are going to be limited. However, the implementation of a partial thermalization model for electrons in the simulation code is far more challenging. The electron fluid model currently implemented in HPHALL-2 (and in other hybrid codes) for the bulk, quasineutral region is based on a one-temperature, quasi-Maxwellian electron distribution. An electron fluid-type model for low thermalization requires to assume (i) a two-temperature distribution for primary electrons. and (ii) an independent distribution for the true-secondary electron beams. This implies, at least, to postulate (i) conditions relating the parallel and perpendicular temperatures of primary electrons, (ii) equations for the macroscopic magnitudes of beam electrons, and (iii) source terms "transforming" beam electrons into primary ones. An additional, important challenge is that the fluid equations for magnetized electrons must be expressed in the non-Cartesian reference frame linked to the curved magnetic streamlines.

Therefore, we believe that there are several important issues related to the evolution of secondary electrons that remain largely unsolved. These should be understood prior to affording the implementation of a new electron model in codes such as HPHALL-2. First, the determination and evaluation of the main physical processes that thermalize (or isotropize) the EVDF are poorly known. Second, Sydorenko *et al.*[28] have shown recently that the two-stream instability can "heat" and trap an important fraction of the secondary beams, thus indicating the existence of a *trapping* process for secondary electrons independent of the *thermalization* of the primary EVDF (modeled through σ). Third, a consistent model for trapped secondary electrons and their "thermalization" into primary electrons (in a slower time-scale) must be derived. Fourth, the fluid model of the secondary beams should take into consideration the different magnetic effects acting on them, such as the $E\times B$ and curvature drifts, magnetic mirror trapping, and the oblique incidence of the magnetic field.

VIII. CONCLUSIONS

A model of the plasma interaction with the dielectric walls of a Hall thruster has been presented. It accounts for partial thermalization of the electron population through a single parameter σ and includes a two-population, four-parameter model for SEE. Analytical expressions are obtained for the main parameters characterizing that interaction, such as the particle and energy fluxes to the walls and sheaths, which are needed as boundary conditions of quasineutral models of the full discharge.

The behavior for low thermalization is shown to differ greatly from the commonly used, high-thermalization case. This is very relevant for Hall thrusters, where there is a growing conviction that electron thermalization is low (at least for primary electrons). At low thermalization, energy losses are close to its minimum, the charge saturation limit is not attainable, and the sheath potential is small; the different roles of beam and primary electrons on these characteristics have been analyzed. Significant decreases of the parallel temperature of primary electrons and, therefore, of the plasma flux into the sheath (through fulfilment of the Bohm condition) take place only at the very-low thermalization limit ($\sigma \ll \sqrt{m_e/m_i}$).

The investigation of the emission model for secondary electrons has shown that the presence of a relevant fraction of elastically reflected electrons affects greatly the response. They tend to amplify the relative densities of untrapped electrons; their effect on the net primary and beam fluxes comes out from the zero electrical current balance. It is reiteratively found that the role of the sheath potential fall is to adjust the primary electron flux to wall and not vice versa. Although most of the analysis is carried out for an energy-independent yield of reflected electrons, a temperature-dependent yield expression is proposed, which avoids integrals expressions at the same time that it recovers approximately the reduction of that yield with the impact energy.

The charge saturation limit is attained when net beam-to-primary net fluxes ratio γ_{bp} is very close to 1, that is, the ratio between the primary-electron-to-ion flux ratio $g_p/g_i \equiv (1-\gamma_{bp})^{-1}$ is very large. The CSL requires larger plasma temperatures as the thermalization decreases and the average yield of reflected electrons increases. Additionally, the sensitivity of the value of g_p/g_i at the CSL to small variations on the model properties has been stood out. As examples we have shown that the influence of a small emission energy of true-secondary electrons (T_2) or the (inconsistent) inclusion of the collected tail of primary electrons are less marginal than what could be expected.

ACKNOWLEDGMENTS

This work was sponsored by the Ministerio de Educación y Ciencia of Spain, under Project No. ESP2004-03093, and by the Air Force Office of Scientific Research, Air Force Material Command, USAF, under Grant No. FA8655-06-1-3032.

APPENDIX: ELECTRON MAGNITUDES IN THE SHEATH

The electron density $n_e(\phi)=\int d\boldsymbol{v} f(\phi,\boldsymbol{v})$ has contributions from primary and beam electrons. Using Eq. (20) for the EVDF and writing $\hat{n}_e=\hat{n}_p+\hat{n}_b$, one has

$$\hat{n}_p(\hat{\phi}) = \mathrm{e}^{\hat{\phi}-\hat{\phi}_\mathrm{Q}}\left[1-\frac{2-(1+\delta_{sr})\sigma\kappa}{2}\,\mathrm{erfc}\sqrt{\hat{\phi}-\hat{\phi}_\mathrm{W}}\right],$$
$$\hat{n}_b(\hat{\phi}) = \frac{\mu_b}{2}\sqrt{\frac{T_1}{T_2}}\mathrm{e}^{-\hat{\phi}_\mathrm{WQ}}\mathrm{e}^{(\hat{\phi}-\hat{\phi}_\mathrm{W})/\hat{T}_2}\,\mathrm{erfc}\sqrt{(\hat{\phi}-\hat{\phi}_\mathrm{W})/\hat{T}_2}, \tag{A1}$$

with $\mu_b \equiv (2-\sigma)(1-\delta_{sr})\kappa\gamma_{bp}$.

The parallel-to-perpendicular temperature ratio of the primary population at point Q, is of interest as well. It is readily seen that the perpendicular temperature is T_1. The temperature ratio $\hat{T}_{rp\mathrm{Q}}$ then satisfies

$$\hat{T}_{rpQ}\hat{n}_{pQ} \simeq \int \frac{m v_r^2 f_{pQ}}{n_1 T_1} d^3v = 1 + \left[(1+\delta_{sr})\frac{\sigma\kappa}{2} - 1 \right] \left(2\frac{\hat{\phi}_{WQ}^{1/2}}{\pi^{1/2}} e^{-\hat{\phi}_{WQ}} + \text{erfc}\ \hat{\phi}_{WQ}^{1/2} \right), \tag{A2}$$

where the integration domain is the whole velocity space and the small contribution of the macroscopic radial kinetic energy of electrons has been neglected.

Using the above expressions for the electron densities, the sonic Bohm condition (37) for $\hat{g}_i$ becomes

$$\frac{\hat{n}_{eQ}^3}{\hat{g}_i^2} = \hat{n}_{pQ} + \hat{n}_{bQ}\frac{T_1}{T_2} + \left[2 - (1+\delta_{sr})\sigma\kappa - \mu_b\frac{T_1}{T_2} \right] \frac{e^{-\hat{\phi}_{WQ}}}{2\sqrt{\pi\hat{\phi}_{WQ}}}. \tag{A3}$$

Finally, the three contributions to the CSL condition,

$$\int_W^Q (\hat{n}_i - \hat{n}_p - \hat{n}_b) d\hat{\phi} = 0, \tag{A4}$$

are

$$\int_W^Q \hat{n}_i d\hat{\phi} = (\sqrt{\hat{g}_i^2 + 2\hat{\phi}_{WQ}\hat{n}_{eQ}^2} - \hat{g}_i)\frac{\hat{g}_i}{\hat{n}_{eQ}},$$

$$\int_W^Q \hat{n}_p d\hat{\phi} = \hat{n}_{pQ} - \hat{n}_{pW} - \frac{2-(1+\delta_{sr})\sigma\kappa}{\sqrt{\pi}} e^{-\hat{\phi}_{WQ}}\hat{\phi}_{WQ}^{1/2}, \tag{A5}$$

$$\int_W^Q \hat{n}_b d\hat{\phi} = (\hat{n}_{bQ} - \hat{n}_{bW})\frac{T_2}{T_1} + \frac{\mu_b}{\sqrt{\pi}} e^{-\hat{\phi}_{WQ}}\hat{\phi}_{WQ}^{1/2}.$$

For $T_2/T_1 \ll 1$ (and $\hat{\phi}_{WQ} \sim 1$), one has

$$\int_W^Q \hat{n}_b d\hat{\phi} \simeq \mu_b e^{-\hat{\phi}_{WQ}} \left(\sqrt{\frac{\hat{\phi}_{WQ}}{\pi}} - \frac{1}{2}\sqrt{\frac{T_2}{T_1}} \right). \tag{A6}$$

[1] V. Zhurin, H. Kaufman, and R. Robinson, Plasma Sources Sci. Technol. **8**, R1 (1999).
[2] A. Morozov and V. Savelyev, *Reviews of Plasma Physics* (Kluwer Academic, New York, 2000), Vol. 21, pp. 203–391.
[3] E. Ahedo, J. Gallardo, and M. Martínez-Sánchez, Phys. Plasmas **10**, 3397 (2003).
[4] G. Hobbs and J. Wesson, Plasma Phys. **9**, 85 (1967).
[5] E. Ahedo, Phys. Plasmas **9**, 4340 (2002).
[6] F. Parra, E. Ahedo, M. Fife, and M. Martínez-Sánchez, J. Appl. Phys. **100**, 023304 (2006).
[7] E. Ahedo, I. Maqueda, A. Antón, Y. Raitses, and N. Fisch, *Proceedings of the 42th Joint Propulsion Conference*, Sacramento, CA (American Institute of Aeronautics and Astronautics, Washington, DC, 2006), Paper No. AIAA-2006-4655.
[8] J. J. Szabo, Ph.D. thesis, Massachusetts Institute of Technology, 2001.
[9] N. Meezan and M. Capelli, Phys. Rev. E **66**, 036401 (2002).
[10] S. Barral, K. Makowski, Z. Peradzynski, N. Gascon, and M. Dudeck, Phys. Plasmas **10**, 4137 (2003).
[11] O. Batishev and M. Martínez-Sánchez, *Proceedings of the 28th International Electric Propulsion Conference*, Toulouse, France (Electric Rocket Propulsion Society, Fairview Park, OH, 2003), Paper No. IEPC-2003-188.
[12] K. Sullivan, J. Fox, O. Batischev, and M. Martínez-Sánchez, *Proceedings of the 40th Joint Propulsion Conference*, Fort Lauderdale, FL (American Institute of Aeronautics and Astronautics, Washington, DC, 2004), Paper No. AIAA-2004-3777.
[13] D. Sydorenko, A. Smolyakov, I. Kaganovich, and Y. Raitses, Phys. Plasmas **13**, 014501 (2006).
[14] S. Fridrikhov and A. Shulman, Sov. Phys. Solid State **1**, 1153 (1960).
[15] N. Bazhanova, V. Belevskii, and S. Fridrikhov, Sov. Phys. Solid State **3**, 1899 (1962).
[16] V. Sizonenko, Sov. Phys. Tech. Phys. **26**, 1345 (1981).
[17] F. Taccogna, S. Longo, and M. Capitelli, Phys. Plasmas **12**, 093506 (2005).
[18] J. M. Fife, Ph.D. thesis, Massachusetts Institute of Technology, 1998.
[19] E. Ahedo and F. Parra, *Proceedings of the 38th Joint Propulsion Conference*, Sacramento, CA (American Institute of Aeronautics and Astronautics, Washington, DC, 2002), Paper No. AIAA-2002-4106; Phys. Plasmas **12**, 073503 (2005).
[20] I. Kaganovich, Y. Raitses, D. Sydorenko, and A. Smolyakov, *Proceedings of the 42th Joint Propulsion Conference*, Sacramento, CA (American Institute of Aeronautics and Astronautics, Washington, DC, 2006), Paper No. AIAA-2006-4831.
[21] E. Ahedo, V. de Pablo, and M. Martínez-Sánchez, *Proceedings of the 29th International Electric Propulsion Conference*, Princeton (Electric Rocket Propulsion Society, Fairview Park, OH, 2005), Paper No. IEPC-2005-118.
[22] E. Ahedo and V. de Pablo, *Proceedings of the 42th Joint Propulsion Conference*, Sacramento, CA (American Institute of Aeronautics and Astronautics, Washington, DC, 2006), Paper No. AIAA-2006-4328.
[23] P. Bhatnagar, E. Gross, and M. Krook, Phys. Rev. **94**, 511 (1954).
[24] V. Viel-Inguimbert, *Proceedings of the 28th International Electric Propulsion Conference*, Toulouse, France (Electric Rocket Propulsion Society, Fairview Park, OH, 2003), Paper No. IEPC-2003-258.
[25] A. Dunaevsky, Y. Raitses, and N. J. Fisch, Phys. Plasmas **10**, 2574 (2003).
[26] A. Morozov, Sov. J. Plasma Phys. **17**, 393 (1991).
[27] V. Kim, V. Kozlov, A. Skrylnikov, L. Umnitsin, V. Svotina, A. Bouchoule, and M. Prioul, *Proceedings of the 29th International Electric Propulsion Conference*, Princeton (Electric Rocket Propulsion Society, Fairview Park, OH, 2005), Paper No. IEPC-2005-004.
[28] D. Sydorenko, A. Smolyakov, I. Kaganovich, and Y. Raitses, Phys. Plasmas **14**, 013508 (2007).